Chapter 4

Accelerator

4.1 Beam Parameters

The major target of JLC has been the center-of-mass energy range of $\sqrt{s}$= 1 to 1.5 TeV and the luminosity around $1\times10^{34}/\mathrm{cm}^2/\mathrm{sec}$ since 1986 when an intensive R&D started. To achieve this goal with a reasonable total length of 25 to 30 km, we have been thinking of the X-band frequency with multiple bunch operation. In the latest parameter set which was reported in LC91, the number of particles per bunch, N, is about 2×10^{10} and the number of bunches per RF pulse, m_b is 20. The recent demand of particle physics, however, puts more emphasis on the relatively low energy range $\sqrt{s}$= 300 to 500 GeV and on earlier start of the experiment around the year 2000.

It is possible that, if we consider these new requirements independently of the previous ones, somewhat different machine might be an optimum. With an observation of the present status of R&D at KEK, in particular if we desire early construction, it seems that the possibility of the frequency range lower than the X-band should also be pursued. Here, we will consider three frequencies, S-band (2856MHz), C-band (5712MHz) and X-band (11424MHz).

The parameter set given in the following is not the one studied fully. It is intended only to serve as the starting point of the design study. It is not intended to decide which frequency is the best. Some parameters are conservative at one frequency but more ambitious at other frequencies. Also, the parameters given here are not necessarily consistent with those referred to in the later chapters. Let us list up the conditions which the parameter set should satisfy.

Global parameters

We assume the active length (the sum of the lengths of the accelerating structures) should be less than 10 km per beam. This will limit the total collider length to about 25 km, including the linac focusing elements and the final focus system. This requirement comes from the availability of the land. (For the S-band at 500 GeV we relax this condition slightly because otherwise it can only be met by unrealistically reducing the number of cavities to be fed by one klystron, which would be quite costly.)

The wall-plug power has to be less than about 200 MW. The above two requirements set an upper limit on the center-of-mass energy. It will be roughly $\sqrt{s}$= 0.5, 1.0, and 1.5 TeV for the S-, C-, and X-band options, respectively, though the latter two call for considerable innovation in the klystron technologies. Here, however, we shall discuss up to 500 GeV only. We set the upper limit of the repetition rate to be 150 Hz.

We set the upper limit for the number of particles per RF pulse to be 8×10^{11}, which is determined by the possible production rate of the positron by an extension of the conventional method. (This limit can be overcome by raising the repetition rate of the positron production linac or by constructing two linacs but these are not practical.)

There is a vast variety of distributing these particles into bunches. Judging from the recent studies of the detuned cavities, we should think of putting more bunches into an RF pulse than the previous value, i.e., 20 bunches. About 100 bunches seem to be possible from the view point of linac beam dynamics and the design of the damping ring. Moreover, Shintake has recently proposed a new-type damped cavity making use of the choke mode. With this cavity many-bunch operations will be quite promising.

We assume that the distance between bunches is 16 buckets for any frequency band. The X-band study has been done with this distance and it turned out that a frequency spread of the TM_1 mode as large as 13% is needed to avoid the multi-bunch beam breakup. A distance shorter than 16 buckets is not practical. So long as we adopt detuned structures, 16 buckets seem to be the lower limit. On the other hand, it might be possible to have longer distance. It consumes some more power and calls for a larger damping ring but is better for multi-bunch energy compensation, the background problem, and the multi-bunch crossing instability.

Main Linac

From the view point of luminosity, a short bunch is preferred because it allows a small beta function at the collision point and because it relaxes the luminosity reduction due to the crossing angle. From the study of the bunch compressor, we set the lower bound of the bunch length to be 80μm. A shorter bunch causes tighter tolerances in the compressor. (Also from the compressor requirement, we set the injection energy to the main linac to be 20GeV.)

The parameters involving the cavity structure, such as the attenuation parameter and the iris aperture, are fixed after some beam dynamics and hard-ware consideration.

The energy spread due to the short range wake is compensated by shifting the bunches off the RF crest. We impose the condition that the resulting peak-to-peak energy spread should be less than 1.5%. Also, we assume that the inter-bunch energy spread due to the transient beam loading can be compensated. When the input pulse shape to the structure is rectangular such as the pulse from SLED II, the energy difference can be compensated almost perfectly by injecting the beam into cavities with various timings of partial fill. If we have, for example, 20 cavities whose timing can be controlled independently, the resulting energy spread can be compensated down to the level of 0.1%. For the S-band, for which SLED II is not practical, the compensation is possible with SLED pulse by using cavities with a small frequency shift. These compensation schemes put a sharp upper bound on $\eta_1 T_f/t_b$ where η_1 is the single-bunch extraction efficiency, T_f the filling time and t_b the bunch spacing. After these compensation, the net accelerating gradient in the structure becomes considerably smaller than the nominal (unloaded) accelerating gradient. We require the reduction to be smaller than 30%. If this is too large, the tolerance of the charge per pulse would become very tight.

Final focus and the interaction point

As for the luminosity, smaller beta functions at the collision point are better because the beamstrahlung is not a serious limiting factor in this energy range. (We define the upper bound of the average energy loss by beamstrahlung $\delta_{BS} \leq 10\%$.) A design study of the final focus system has concluded that $\beta_x \geq$10mm and $\beta_y \geq$0.1mm are possible within reasonable tolerances.

We assume a horizontal crossing with a crossing angle larger than 5mrad. This is needed in order to let the exhaust beams go outside the field region of the last quadrupole magnet. The bunches coming late are deflected by the exhaust bunches (multi-bunch crossing instability). We require the amplitude blowup factor by this instability to be less than 2. Actually, this requirement calls for a crossing angle larger than 5mrad and, therefore, the luminosity is somewhat reduced by the geometric reduction factor and by the reduction of the pinch enhancement factor. The so-called crab crossing can cure this problem. The luminosity would become larger by a factor of 1.5 to 2 but we do not take this option here.

With the consideration above, we determined the parameters which makes the luminosity as high as possible and listed them in Table 4.1. (We also included possible parameters at the Z_0 energy for C-band only.)

The luminosity only is, however, not a good parameter to be optimized. In fact, there are many different solutions which give nearly the same luminosity (e.g., different combinations of N and m_b). Also, we prefer a smaller beam energy spread in some experiments, which changes the optimization considerably. The table here gives only one possible set for each frequency. To decide which solution of which frequency is the best, we need many steps of iteration between the global design and those of each part.

4.2 Electron and Positron Sources

4.2.1 Electron source

Introduction

The electron source of JLC-I must be able to produce 55 $\sim$ 90 intense electron bunches separated by a spacing depending on RF band selection(1.4 ns for X-, 2.8 ns for C-, and 5.6 ns for S-band) with a repetition rate of 50 or 150 Hz as illustrated schematically in Fig. 4.1. Each bunch consists of 0.7$\sim$ 1.5 $\times$ 10^{10} electrons. The resultant total number of electrons is 6 $\sim$ 8 $\times$ 10^{11}/RF pulse. The number of electrons in each bunch must be controlled to better than $\pm$0.5 % and its emittance must be small enough to be accepted in the pre-damping ring as described in Sec. 4.3.

To meet these requirements, we take the following two approaches: one is to push, to the limit, the conventional technology using a pulsed thermionic gun combined with a grid pulse generator and sub-harmonic bunchers(SHB), and the other is to develop an RF gun with a laser-triggered photocathode.

Effort is also made to develop a highly polarized electron source which will be discussed in Sec. 4.2.2.

Thermionic Gun

a) Single and double bunch generation : As the first step of the development program, single- and double-bunch beams were studied to confirm the feasibility of achieving the required number of electrons per bunch. In this study, we used fast pulse generators to produce grid pulses to drive the thermionic cathode. The pulse generators were originally built by Kentech

Table 4.1: Parameters at E_{CM}=300 and 500 GeV

			S-band		C-band		X-band		C-band
Frequency	f_{rf}	GHz	2.856		5.712		11.424		5.712
Beam Energy	E	GeV	150	250	150	250	150	250	45.6
Number of Particles per bunch	N	10^{10}	1.73	1.45	1.11	1.10	0.70	0.70	1.11
Number of bunches per pulse	m_b		46	55	72	72	90	90	72
Bunch spacing	t_b	nsec	5.6	5.6	2.8	2.8	1.4	1.4	2.8
Repetition frequency	f_{rep}	Hz	50	50	150	150	150	150	150
Normalized emittance at damping ring	ε_x	rad.m	3×10^{-6}	3×10^{-6}	3×10^{-6}	3×10^{-6}	3×10^{-6}	3×10^{-6}	3×10^{-6}
	ε_y	rad.m	3×10^{-8}	3×10^{-8}	3×10^{-8}	3×10^{-8}	3×10^{-8}	3×10^{-8}	3×10^{-8}
R.m.s. bunch length	σ_z	μm	80	80	80	80	85	67	80
Nominal accelerating gradient	G_0	MeV/m	22.0	22.0	40.0	40.0	40.0	40.0	40.0
Effective gradient in cavities	G_{eff}	MeV/m	16.3	18.4	28.2	27.8	28.0	28.0	28.5
Active length of main linac per beam	L_{ac}	km	8.0	12.5	4.6	8.3	5.0	8.5	0.90
Total number of betatron oscillation			200.	258.	116.	171.	125.	176.	33.5
Length of a cavity unit	l_{cav}	m	3.6	3.6	1.7	1.7	1.22	1.22	1.7
Number of cavity units per beam			2220	3470	2720	4860	4100	6930	530
Iris radius/Wave length	a/λ		0.12	0.12	0.13	0.13	0.18	0.18	0.13
Cavity filling time	T_f	nsec	837	837	297	297	75	75	297
Attenuation parameter	τ		0.57	0.57	0.57	0.57	0.40	0.40	0.57
Total average power into cavities for two linacs		MW	14	20	25	46	11	20	5.0
Wall-plug power for two linacs		MW	70	100	115	210	75	135	23
Assumed efficiency from AC to RF		%	20	20	22	22	15	15	22
Peak power per cavity	P_{peak}	MW	52	52	60	60	50	50	60
Single-bunch extraction efficiency	η_1	%	0.84	0.70	1.13	1.13	2.00	2.00	1.13
Phase shift from the crest	ϕ_{rf}	deg	28.0	11.0	21.9	23.9	24.0	24.0	21.6
Single-bunch energy slope due to wake	$\langle\sigma_z d\epsilon/dz\rangle$	%	-0.72	0.57	-0.84	-0.90	-1.22	-1.22	-0.54
Energy slope for BNS damping		%	-0.008	-0.007	-0.06	-0.06	-0.16	-0.16	-0.06
Number of particles per bunch at IP	N^*	10^{10}	1.56	1.30	1.00	1.00	0.63	0.63	1.00
Beta function at IP	β_x^*	mm	10.	10.	10.	10.	10.	10.	10.
	β_x^*	μm	100.	100.	100.	100.	100.	100.	150.
Rms beam size at IP	σ_x	nm	335	301	335	260	335	260	608
	σ_y	nm	3.92	3.04	3.92	3.04	3.92	3.04	8.70
Crossing angle	ϕ_{cross}	mrad	11.0	7.3	10.4	8.0	9.0	7.2	15.1
Beam diagonal angle	σ_x/σ_z	mrad	4.2	3.8	4.2	3.2	4.0	3.9	7.6
Disruption parameter	D_x		0.21	0.13	0.13	0.13	0.090	0.0070	0.135
	D_y		18.0	13.0	11.5	11.5	7.7	6.0	9.41
Number of beamstrahlung photons	n_γ		1.80	1.62	1.19	1.44	0.80	0.95	0.71
Maximum Upsilon	Υ_{max}		0.37	0.58	0.24	0.51	0.15	0.39	0.041
Energy loss by beamstrahlung	δ_{BS}	%	8.2	10.0	3.9	8.1	1.8	4.5	0.46
Geometrical luminosity reduction factor			0.57	0.68	0.60	0.60	0.63	0.70	0.69
Pinch enhancement factor	H_D		1.58	1.60	1.50	1.50	1.71	1.72	1.80
Luminosity	L	10^{33}/cm^2/s	3.1	4.4	5.9	9.7	3.5	6.3	2.0

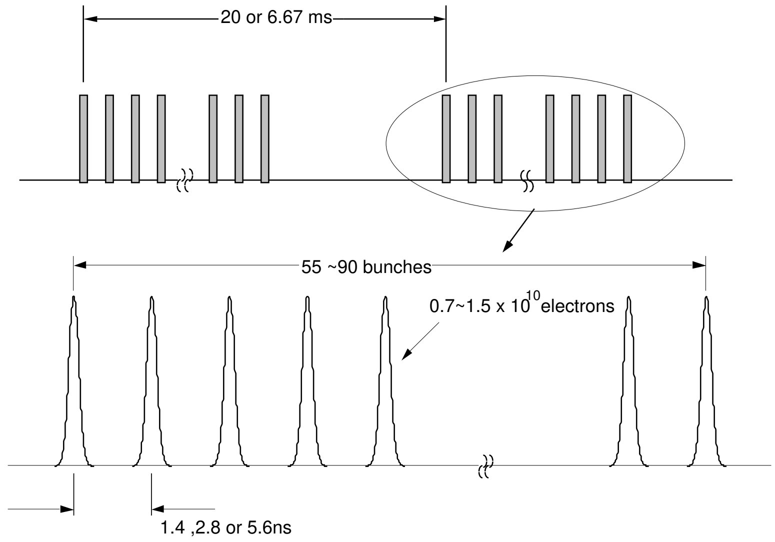

Figure 4.1: Schematic drawing of the electron and positron beam.

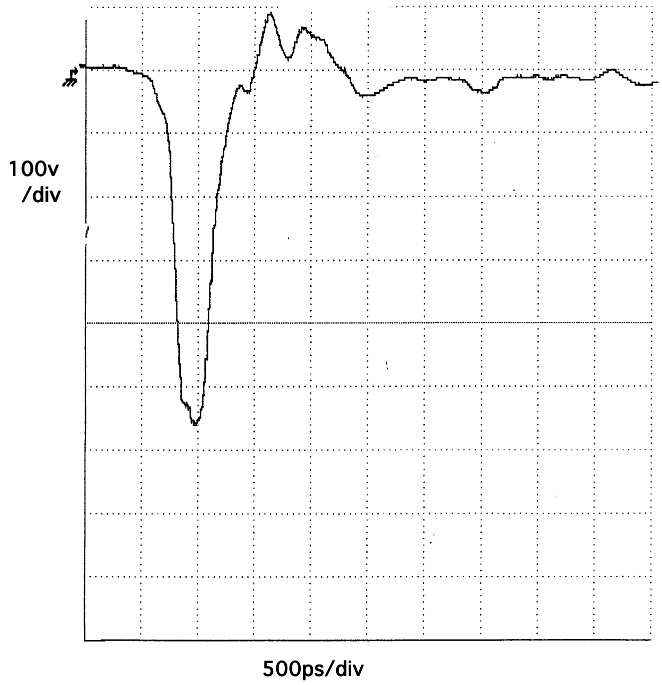

Figure 4.2: Output of the fast avalanche pulse generator (100 V/div, 500 ps/div).

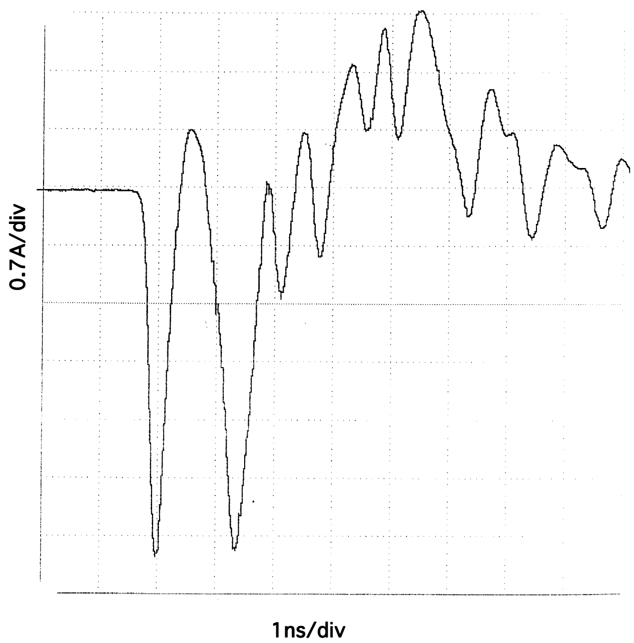

Figure 4.3: Wave shape of double bunch beam, accelerating voltage: 170 kV, heater voltage: 6.0 V, net drive voltage: 260 V

Instruments Ltd, which employ avalanche transistor pulse generator technology. A typical pulse shape is shown in Fig. 4.2. The peak pulse amplitude and the width were $\sim$ 500 V and 500 ps. The double grid pulses required for double-bunch generation were formed by using two avalanche pulse generators, triggered at different timings, and delivering their output pulses to an RF combiner. The peak amplitude and the width of each pulse from the RF combiner were $\sim$ 300 V and 500 ps, respectively. The reduction of the amplitude was due to the power loss in the RF combiner. Fig. 4.3 shows a typical double-bunch beam from the Y-646 cathode driven by the double grid pulses, where the accelerating voltage was 170 kV, the heater voltage 6.0 V, and the net drive voltage 260 V. The peak current of each bunch was 4.3 A which corresponds to 1×10^{10} electrons/bunch. Although this value already reached the required single-bunch intensity, generation of more than several bunches is difficult with this pulse generation system because of the power loss in the RF combiner.

b) Multi-bunch generation : A new multi-pulse generator under development uses a fast ECL circuit and an RF amplifier to generate more than 20 pulses per train. Fig. 4.4 shows its schematic diagram. The ECL clock is 476 MHz synchronized to the RF of the linac. Required number of pulses are successfully formed by counting and gating the RF signals in the circuit, as shown in Fig. 4.5(a). The RF power amplifier is required to have an output power of $\sim$10 kW and a gain of 60 dB to provide sufficiently large pulses to drive the gun. The band width of such a high gain RF amplifier is not large enough to amplify this pulse train with no distortion, as shown in Fig. 4.5(b) for a 1 W test RF amplifier. The distortion can be cured by a compensation signal from the wave form shaper. Since there is no foreseen technological problem with high power RF amplification, we are confident that this new scheme will meet the JLC requirements.

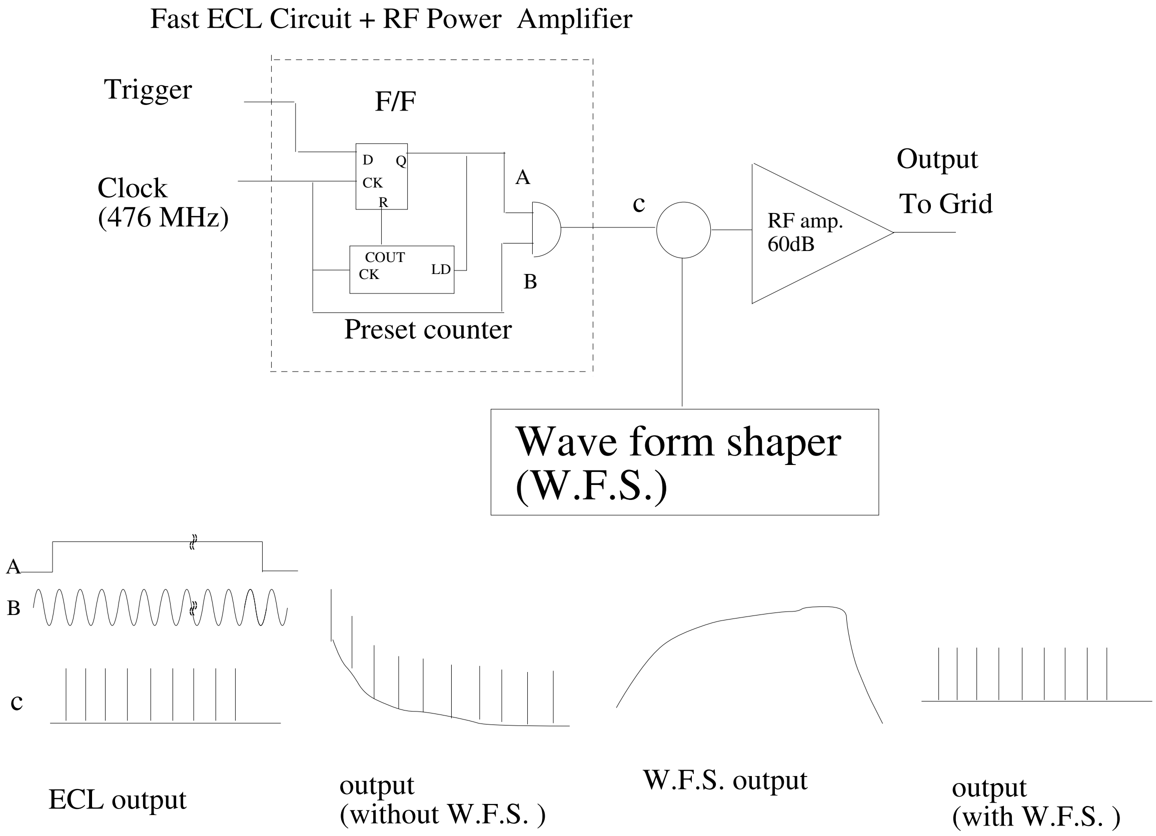

Figure 4.4: Schematic drawing of multi-pulse generator.

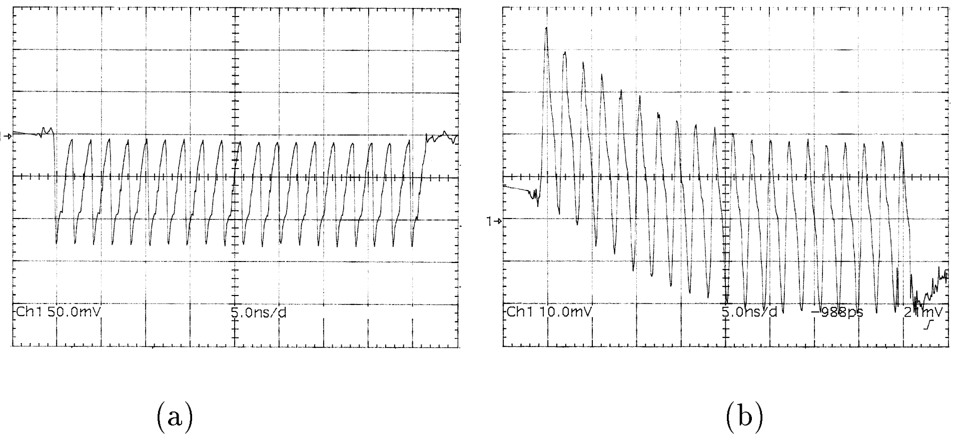

(a) (b)

Figure 4.5: (a) Output of the fast ECL circuit (50 mV/div, 5 ns/div) and (b) Output of the test RF amplifier (1.5 V/div, 5 ns/div)

c) Test Facility : The thermionic gun described above has been installed into the first stage accelerator test facility shown in Fig. 4.6, which includes three SHBs(119/238/476 MHz), two single-cell pre-bunchers, and a traveling wave S-band buncher followed by a high gradient S-band accelerating structure. The test facility made possible systematic studies of the electron source system and proved its capability of stably delivering at least 1×10^{10} electrons/bunch to the injector linac. This source system will be used for single-bunch studies of various components in the full Accelerator Test Facility(ATF) including a chain of a 1.5 GeV injector linac, a low-emittance damping ring, and a bunch compressor.

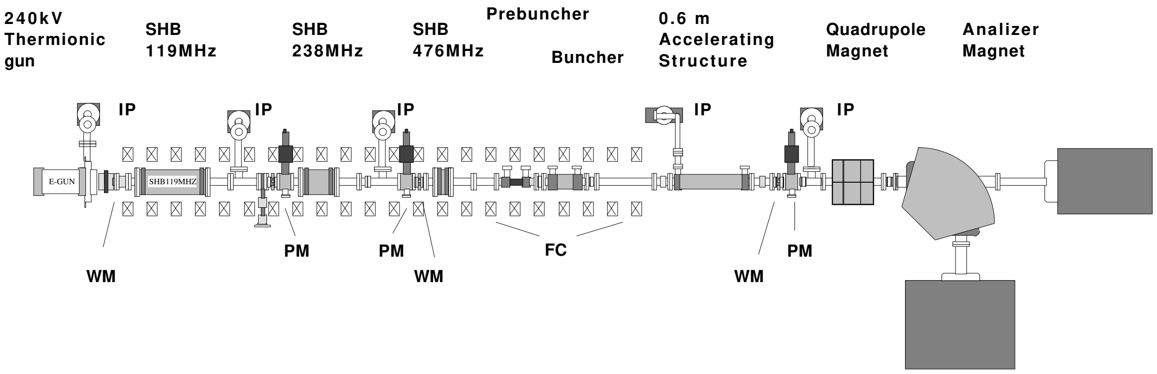

Figure 4.6: Layout of the Accelerator Test Facility.

RF Gun

An RF gun using a laser-triggered photocathode has many advantages in generating a low emittance and high current pulsed beam. The RF gun directly generates a bunched beam by illuminating, with laser pulses, a photocathode installed in an RF cavity. The RF field accelerates the bunch in synchronization with the laser pulses as illustrated in Fig. 4.7. The

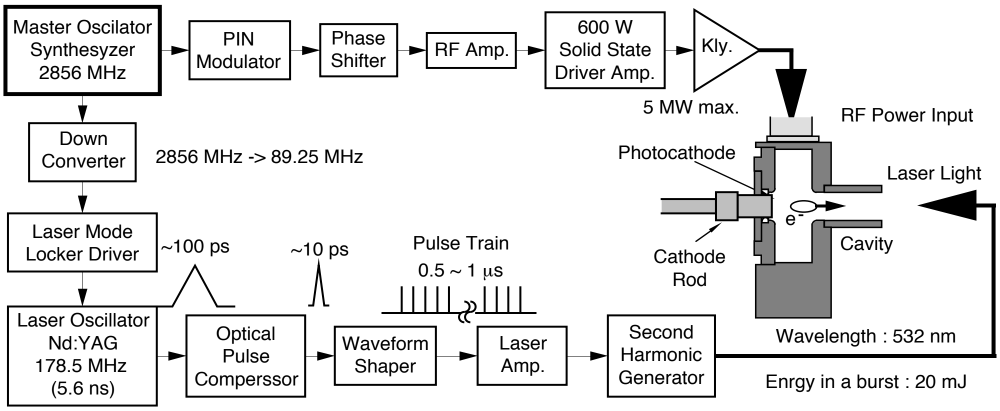

Figure 4.7: A schematic drawing of the RF gun.

accelerating gradient achievable with the RF field is higher than that of a DC or pulsed field of the conventional gun, so that it is possible to generate an extremely low emittance and high current beam. Since the photocathode is triggered with a pulsed laser, the required pulsed beam can be produced only using a mode-locked laser system and an optical system. Furthermore, compared to the thermionic gun, higher current density is achievable. Motivated by these good characteristics, we are devoting a great deal of effort to the development of a RF gun system which meets the requirements for JLC-I.

a) Prototype RF Gun : Fig. 4.8 shows the experimental facility constructed to study the feasibility of the RF gun. The facility consists of a prototype RF gun with a photocathode in a simple half-cell S-band pillbox-type cavity, a beam transport leading to a current monitor, a mode-locked Nd:YAG laser system, and a high power and low level RF systems.

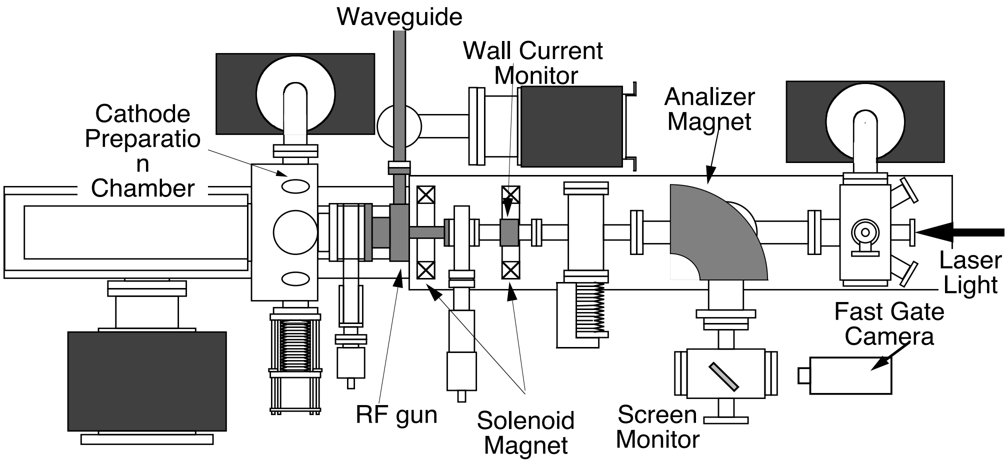

Figure 4.8: An experimental arrangement of the prototype RF gun.

Photocathode : We have chosen the Sb-alkali(Cs) photocathode, whcih is expected to have a high quantum efficiency(Q.E.) for a laser wavelength around 500 nm and is easy to fabricate.

Cavity : In the present experiment, a simple pill-box type cavity is chosen to study the beam dynamics in the RF gun at a high accelerating gradient. The cavity has been processed up to the accelerating gradient of 50 MV/m prior to the experiment. During the experiment at 40 MV/m, no RF breakdown was observed and the vacuum pressure in the cavity was around 1×10^{-9} Torr.

Phase Stability : In the RF gun, the phase between laser pulses and the RF fields must be synchronized precisely. As shown in Fig. 4.7, the master oscillator is an S-band synthesizer. Its output is simply scaled down to 89.25 MHz to trigger the laser and, in this way, phase jitter can be reduced to less than 10 ps.

Laser : A block diagram of the laser system is given in Fig. 4.9. The oscillator is a CW mode-locked Nd:YAG laser with the wavelength of 1064 nm, a power level of 4 W, and the frequency of 178.5 MHz which corresponds to the pulse spacing of 5.6 ns. The width of each pulse is about 100 ps at the output of the oscillator, and is compressed to about 10 ps with an optical pulse compressor composed of an optical fiber and a pair of grating. A pulse train

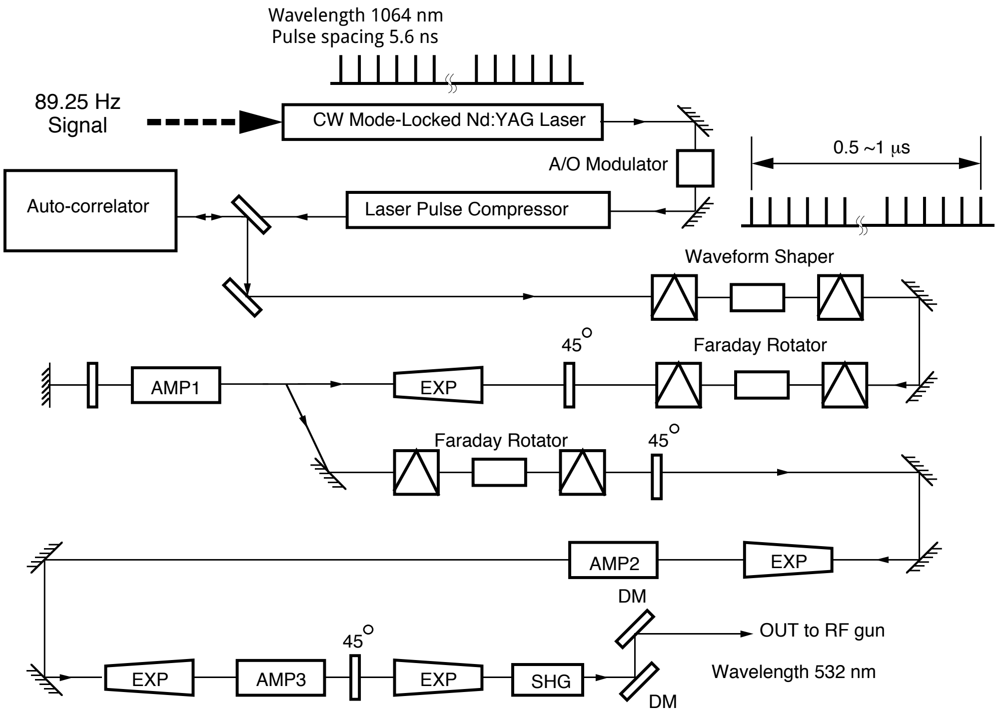

Figure 4.9: A block diagram of the laser system and a picture of a laser pulse.

of 0.5$\sim$ 1 μs in width is obtained from the CW laser pulse with a wave form shaper and then amplified. Finally, the wavelength is converted to 532 nm with a second harmonics generator(KD*P) and the laser light is guided to the photocathode in the cavity with the mirror system. The energy of the one micro-pulse is 0.1 $\sim$ 0.15 mJ.

b) Prototype Tests and Perspectives : Firstly, the photocathode is activated in the preparation chamber and then inserted to the cavity to tune the resonant frequency at 2856 MHz. The laser is fired and the pulse shape of the beam current is observed by the wall current monitor. Fig. 4.10 shows that the beam has the bunch spacing of 5.6 ns, which is precisely the mode locked frequency of the laser system. The number of electrons contained in a pulse was estimated to be 2.3×10^{10} and the number of bunches in one RF pulse was 90$\sim$180. The maximum beam energy was measured with a magnetic spectrometer to be 900 keV at the gradient of 40 MV/m. These experimental results almost satisfy the required performance for JLC-I. The remaining problems are now confined to the improvements of (1) the quantum efficiency and life time of the Cs_3Sb photocathode and (2) the stability and life time of the laser system. The cathode life is determined by the desorption of Cs and the contamination by bad gases such as H_2O and CO. The improvement of the vacuum system is under way, as well as the development of new methods to supply Cs continuously to the cathode during the operation. The flash lamp of the laser system should be replaced by the laser diode to improve both the stability and life time.

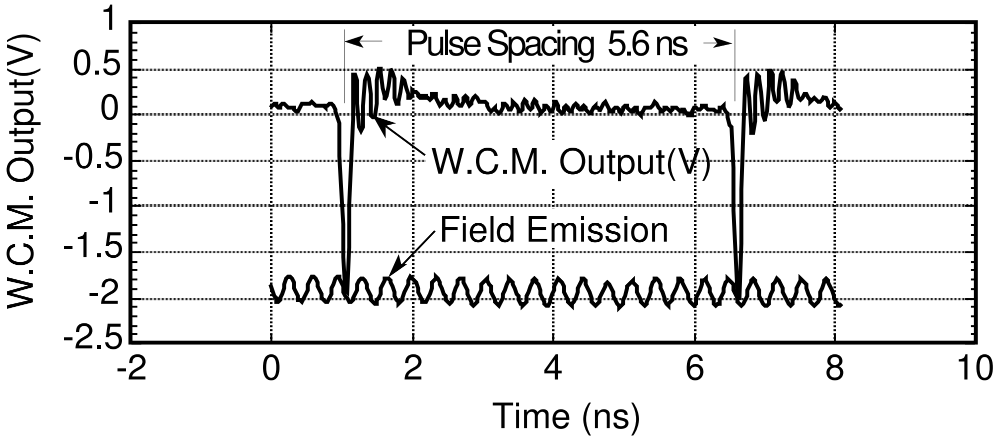

Figure 4.10: Output pulse from the RF gun measured by a wall current monitor.

4.2.2 Polarized Electron Source

In circular e^+e^- colliders, the beams spontaneously polarize vertically due to the spin-flip synchrotron radiation. It calls for tremendous efforts, however, to rotate the spin to the longitudinal direction without serious depolarization. One of the advantages of the linear colliders is that it is relatively easy to collide longitudinally polarized beams once polarized particle sources are given. Polarized positron sources are not easy to obtain but a polarization of one of the beams can already bring about rich physics outputs.

We have made an effort to develop a highly polarized electron source using a GaAs photocathode illuminated by circularly polarized laser light. As is well known, the polarization obtainable with conventional bulk GaAs has an intrinsic upper limit of 50 % due to the symmetrical structure of the crystal. To overcome this limit, we have been studying two types of cathodes, an AlGaAs-GaAs superlattice and a strained GaAs.

In order to develop such GaAs sources, we proceeded with the following two R/D works,
a) photocathode development toward the 100 % polarization,
b) construction of an operational gun which meets the requirements from the JLC injection linac.

Photocathode Development

We have achieved the polarization of 71% and 86% by developing the newly designed photocathodes, GaAs-AlGaAs superlattice and lattice-mismatched strained GaAs, respectively[1, 2]. SLAC group has also achieved 71% from strained InGaAs[3]. These achievements were the break-through to overcome the 50 % polarization limitation of the traditional GaAs source.

The strained GaAs photocathode was made by growing a GaAs epilayer on a lattice mismatched GaP_xAs_{1-x} buffer substrate with a MOCVD apparatus. The structure of prepared samples is simple as shown in Table 4.2. The polarization(ESP) and quantum efficiency(QE) observed for the first successful strained GaAs photocathode are plotted in Fig. 4.11, as a function of laser wavelength. The clear polarization peak at $\lambda \approx 860$ nm is the evidence for the single excitation from the upper heavy-hole band of the strained GaAs. With this sample, the world highest ESP of 86 % was achieved, which was the first proof of the principle to obtain more-than-50 % polarization. However, there still remains another problem, that is

Table 4.2: Parameters of strained GaAs cathode

Zn-doped GaAs ($t \approx$Å, $p \approx 5 \times 10^{18}$cm^{-3})
Zn-doped GaP$_x$As$_{s1-x}$ (x $\approx$ 0.17) (t$\approx$ 2μm, p$\approx 5 \times 10^{18}$cm^{-3})
Zn-doped GaAs Subtrate (t$\approx$ 350μm, p$\approx 5 \times 10^{18}$cm^{-3}) Orientation : (1 0 0)

the relatively poor QE for the new cathodes. For example, the QE was 0.02 % for the above sample at $\lambda \approx 860$ nm, where the maximum ESP of 86 % was observed, while a QE more than 3 % is possible for the bulk GaAs photocathode. We have been trying to improve the quantum efficiency and have achieved so far a more-than-0.1 % QE at 80 % ESP.

The other photocathode of GaAs-AlGaAs superlattice(SL) was fabricated by a MBE apparatus. In Fig. 4.12, the maximum ESPs for 4 samples are plotted as a function of the SL thicknesses, 0.05, 0.1, 0.4 μm[4]. The clear thickness-dependence of ESP confirmed that the depolarization process inside the SL plays a dominant role to degrade the ESP of conduction electrons before they can escape to the vacuum. We also studied the dopant-concentration dependence of the EPS and the QE. It was found that reduced doping was able to lower the spin relaxation in the interior of the superlattice and improve both the EPS and the QE[5]. The best photocathode so far achived gave the 0.2% QE at the 71.2% ESP.

Design and Construction of an Operational Gun

The level of required performance for JLC-I is much higher than those of the previously employed, although the GaAs source was already operated at several laboratories for high energy experiments. It is especially true for the performance under high voltage(100 $\sim$ 200 kV) and the photocathode performance under high power laser irradiation(30 $\sim$ 100 kW peak power).

In order to investigate the above two problems, proto-type guns were constructed both at KEK and Nagoya University. The polarized electron source system build at KEK is shown in Fig. 4.13, where the polarization measuring system, a Wien filter, and a Mott analyzer are also included.

The mechanical construction has been completed and test operation is in progress at moderate high voltage with a moderate power Ti:Sapphire tunable laser system. The vacuum has no problem, already reaching the base pressure of 2×10^{-10} Torr(total pressure), and the initial high voltage up to 100 kV sees no serious dark current. A photocurrent has already been extracted and studies of photocathode performance will start soon. The gun will then be tested with a newly upgraded high-voltage and laser system, which meets the conditions required by the JLC-I injection linac. The first acceleration of polarized electrons at KEK is scheduled in (2 $\sim$ 3) years at the ATF which is under construction.

Acceleration of the polarized beam

Once a polarized source is given, what is needed next is to maintain the high polarization during the acceleraton and to rotate the spin to the longitudinal direction at the collision point.

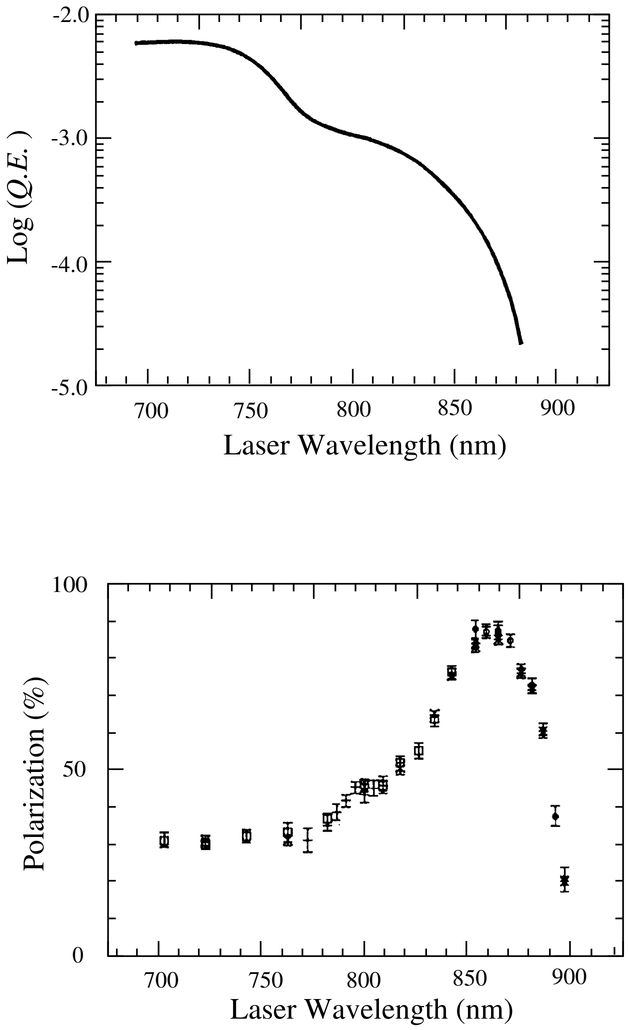

Figure 4.11: Polarization and quantum efficiency for strained GaAs versus laser wave length.

The spin in the damping rings has to be vertical. Otherwise, the beam is immediately depolarized by the precession-frequency spread due to the energy spread. Spin rotators before damping rings for this purpose can easily be designed, since a high beam quality is not required at this stage. The depolarization in the ring is then negligible unless the precession resonates with the revolution frequency or with the betatron frequencies. Since the spin tune (number of precessions during one turn) is simply given by the beam energy divided by $E_r \equiv mc^2/a =$ 440 MeV, where m is the rest mass and a the coefficient of the anomalous magnetic moment, the resonances can be avoided by choosing the beam energy to be 440 MeV times a half odd integer. In fact, our design energy 1.98 GeV was selected in this way. This is the safest choice but one need not strictly obey this rule because the resonance widths are expected to be very small.

In the main linac, the spin must be in the horizontal plane and point towards a definite direction which is determined by the bending angle in the final focus system and by the beam energy after the linac. Thus, we need a spin rotator somewhere between the damping ring and the main linac.

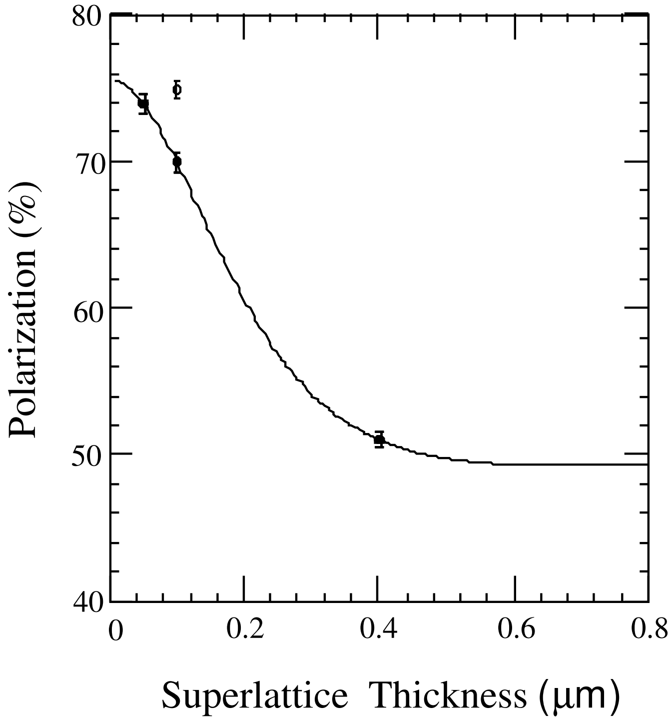

Figure 4.12: Polarization for GaAs-AlGaAs as a function of the superlattice thickness.

If a horizontal polarization can survive in the second bunch compressor, the best location for the spin rotation will be between the first compressor and the pre-linac because the spin manipulation is easier at lower energies. The second compressor consists of a cavity (frequency f_1=11.4 GHz, peak voltage V_1=534 MV) and an arc with the bending angle 180 degrees (including the sign), followed by another cavity and a chicane scheme (see Sec. 4.4). The depolarization in the chicane is negligible because the net bending angle is zero. The particle energy in the first arc is given by

$$E = E_0 + \Delta E - \alpha z/\sigma_z, \qquad \alpha = 2\pi f_1 V_1 \sigma_z / c = 46\text{MeV}, \tag{4.1}$$

where E_0=20 GeV is the average energy, ΔE and z the energy deviation and the longitudinal position of the relevant particle at the exit of the pre-linac, and σ_z the rms bunch length. The precession angle in the first arc is given by $\pi E/E_r$. By assuming a uniform distribution for ΔE over $\pm\Delta E_{max} = \pm 0.57\% \times E_0$ and a Gaussian distribution for z, one finds the reduction factor of the horizontal polarization to be

$$\sin\phi_{max}/\phi_{max} \exp[-(\pi\alpha/E_r)^2/2] = 0.89 \times 0.95 = 0.85, \qquad (\phi_{max} = \pi\Delta E_{max}/E_r). \tag{4.2}$$

Thus, the depolarization in the second compressor is significant if the polarization is in the horizontal plane. Therefore, the spin has to be vertical in the second compressor and must be rotated before injection to the main linac. The rotator to this end has not yet been designed but is believed to be feasible. It inevitably contains either solenoids or vertical bends. Therefore, the increase of the vertical emittance has to be studied carefully.

Since the trajectory in the linac is almost straight, the depolarization there is negligible. The depolarization in the final focus system can come from the horizontal bends but is very small (<0.2%).

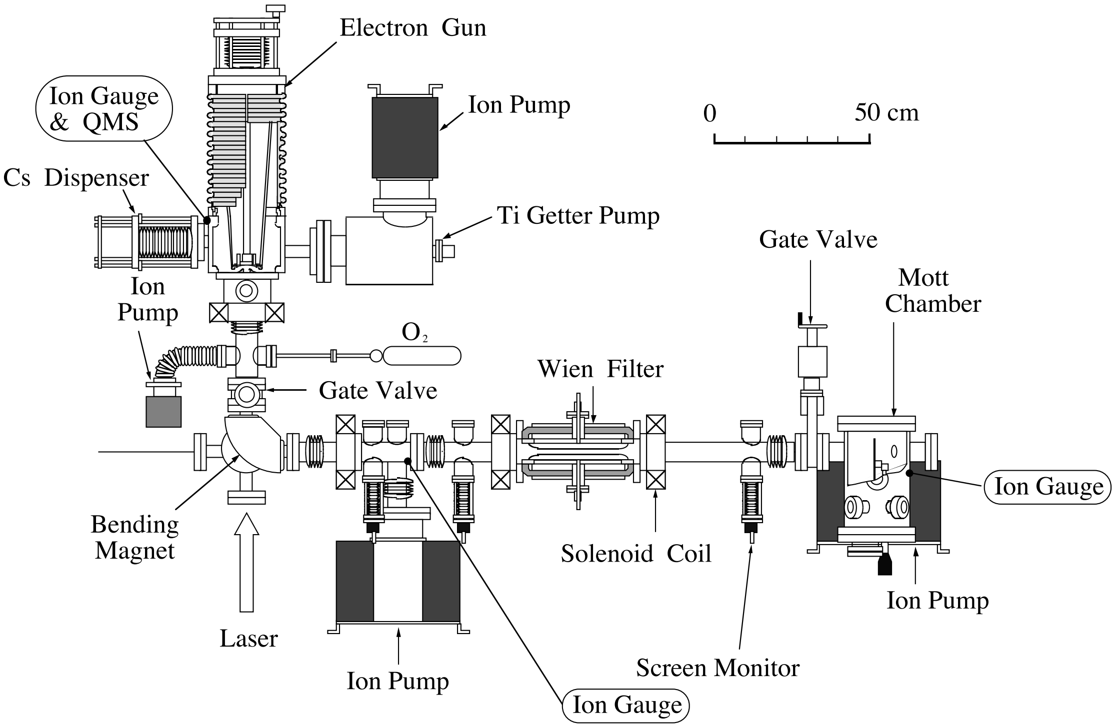

Figure 4.13: An apparatus of polarized electron source.

Finally, the depolarization during the collision has to be examined [6]. In our energy region, where Υ, the ratio of the critical energy of the beamstrahlung to the beam energy, is less than unity, the depolarization due to precession in the beam-beam field is estimated to be $0.006n_\gamma^2$, where n_γ is the number of photons per electron. Since n_γ does not exceed 1.8 (see Sec. 4.1), this depolarization is less than 2%.

At high energies, there is another mechanism of depolarization, namely, the spin-flip synchrotron radiation. The depolarization can be estimated by $2n_\gamma F(\Upsilon)$, where $F(\Upsilon)$ is the ratio of spin-flip to non-flip transition rates. In our region of 300 GeV to 500 GeV, the average of Υ ($\sim \Upsilon_{max}/2.4$) ranges beteeen 0.06 and 0.25, and F between 6×10^{-4} and 4×10^{-3}. Thus, the depolarization due to the spin-flip is at most 1.5%. When Υ is much smaller than unity, F is approximated by $(7/24)\Upsilon^2$. Therefore, the spin-flip depolarization is totally negligible in the Z^0 region.

Note that these values of the beam-beam depolarization are those through the whole process of the collision. The average depolarization during the collision will be about one quarter to one third of them. Also note that the above estimates have some ambiguity due to the disruption and the unknown detail of the bunch shape before collision. If an accurate value of the polarization is needed, one has to measure the polarizations before and after the collision, from which one can evaluate the average polarization during the collision possibly with an accuracy better than $\sim$1%.

4.2.3 Positron Source

The JLC-I positron source should be able to produce an intense positron beam of $7 \sim 15 \times 10^9$ particles per bunch and $55 \sim 90$ bunches per RF-pulse, as shown in table 4.3, so that our goal for positron production was set to 8×10^{11} positrons per RF-pulse. In this subsection, we will show how to achieve this goal with the conventional positron production method, which exploits electromagnetic cascade showers initiated by high-energy electrons injected on a converter target. Since the thermal stress limits the total acceptable energy by the converter target, we cannot simply increase the number of electrons or the incident energy or both, to meet the JLC-I requirement. We also need to increase the positron capture efficiency as high as possible, by introducing a pre-damping ring which has a large transverse acceptance. The design of such a positron source involves a complicated optimization of various parameters, which necessitates systematic simulation studies. We first define the problem more explicity and then describe the solution obtained from the simulation studies.

Table 4.3: Positron source related parameters of JLC-I (Tentative)

The center of mass energy[GeV]	300	500
Number of particles per bunch	6.3×10^9	6.7×10^9
Number of bunches per rf-pulse	98	102
Repetition rate[Hz]	150	150
Bunch spacing [ns]	2.8	2.8

Statement of the Problem

The positrons emerging from the production target are captured and accelerated to the pre-damping. The number of positrons N_+ accepted by the pre-damping ring is roughly proportional to the energy E_- and the number N_- of incident electrons,

$$N_+ = N_- E_- \eta, \tag{4.3}$$

where η is the positron production and capture efficiency. The thermal stress limit ρ on the energy density of the incident electrons was obtained at SLC[7, 8] as

$$\rho = \frac{N_- E_-}{\pi \sigma^2} \leq 2.0 \times 10^{12} \mathrm{GeV/mm^2}, \tag{4.4}$$

where σ is the rms beam radius. The efficiency η is roughly proportional to the accepted normalized emittance ϵ of the pre-damping ring and the beam transport system, and inversely proportional to the rms beam radius,

$$\eta \propto \frac{\epsilon}{\sigma}. \tag{4.5}$$

Therefore, the number of positrons accepted by the pre-damping ring satisfys

$$N_+ \propto \epsilon \sigma \rho, \tag{4.6}$$

when we operate the target at its thermal stress limit. Since ρ cannot be increased drastically with a conventional metal target, we need to increase ϵ and σ. We can increase σ as long as the beam power given by Eq. 4.4 is manageable. As for ϵ, we should increase the tranverse acceptance of the transport system including a S-band linac, so as to match that of the pre-damping ring, which has an acceptable normalized emittance of 0.027 rad $\cdot$ m.

Positron Production System

A schematic diagram of the JLC-I positron-production system is given in Fig. 4.14. The phase-

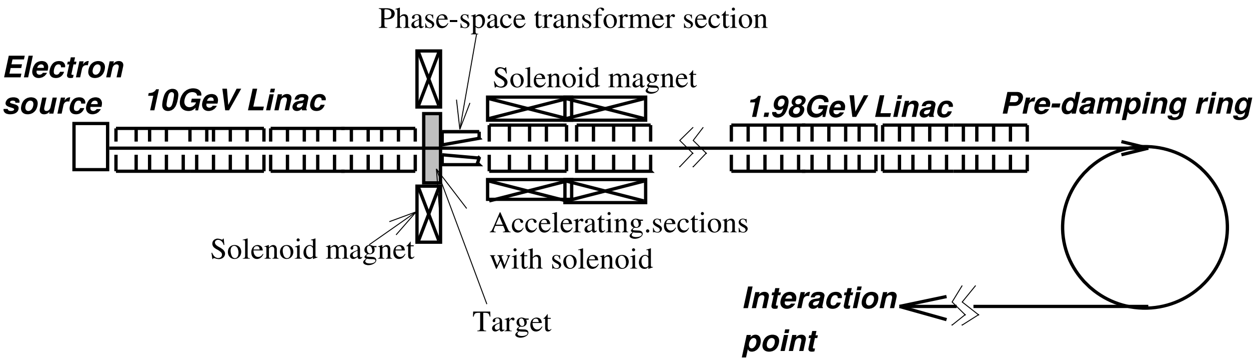

Figure 4.14: A schematic diagram of the positron source for the JLC.

space transformer section, called an adiabatic device[9], just after the target is to accomplish a large radial and energy acceptance. It produces a slowly varying magnetic field along the beam axis, with a flux concentrator[10]. The positrons emerging from the phase-space transformer section are accelerated up to 100 MeV in the accelerating sections surrounded by a long solenoidal magnet. They are then transported to a 1.98 GeV linac leading to the pre-damping ring. In the optimization of various parameters of the positron source system, we have used the EGS4[10] for shower simulations and the Runge-Kutta method for the tracking through the phase-space transformer and the accelerating sections.

Injected Electron Beam : Figure 4.15 gives the simulated positron intensity and the required beam power on the target as a function of the incident beam radius. If we set the rms beam radius to 1.2 mm, 9×10^{11} electrons per RF-pulse can be injected at an incident energy of 10 GeV, resulting in more than 1×10^{12} positrons/RF-pulse. Our goal is to produce 8×10^{11} positrons/RF-pulse which requires 5.4×10^{11} electrons. This intensity corresponds to a beam power of 130 kW on the target, which is 4.5 times higher than that of SLC.

Target Section : W-Re is a suitable material for the converter target because of its high melting point and good fabrication property. Figure 4.16 gives the simulated positron intensity at the interaction point and the rms beam radius at the exit of the target as a function of target thickness for the incident electron energy of 10 GeV. The positron intensity increases linearly with the converter thickness up to 6 radiation lengths(X_0), so that the 6 X_0 appears optimum.

Phase-space Transformer Section : Positrons emerging from the target have large transverse momenta of around 3 MeV/c and, therefore, should be transformed in phase-space by an adiabatic device, to be acceptable for downstream accelerating sections. The longitudinal component of the magnetic field in the adiabatic device is given by

$$Bz = \frac{Bi}{1 + \mu z}, \tag{4.7}$$

where Bi is the initial magnetic field at the target exit and μ is a constant depending on the device. Figure 4.17 shows the simulated positron intensity as a function of Bi. It appears

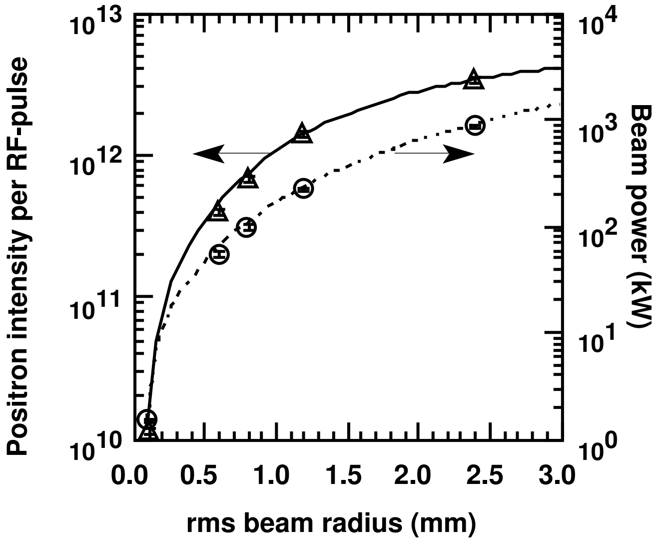

Figure 4.15: The simulated positron intensity and the required beam power on the target as a function of the incident beam radius.

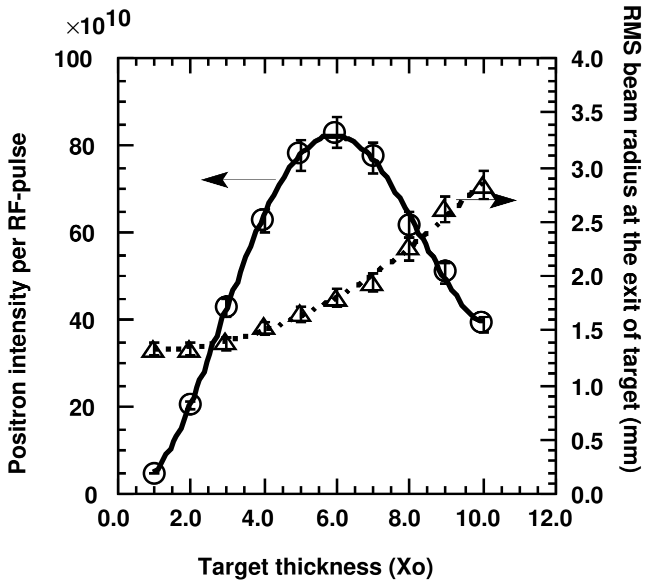

Figure 4.16: The simulated positron intensity at the interaction point and the rms beam radius at the exit of target as a function of target thickness for the incident electron energy of 10 GeV.

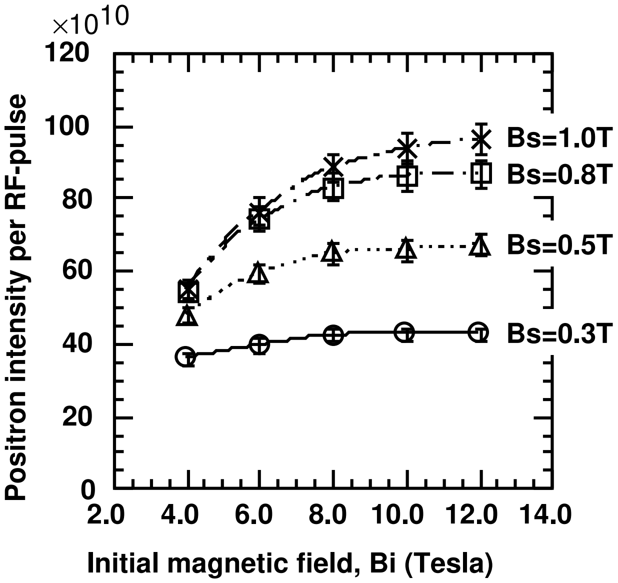

Figure 4.17: The simulated positron intensity as a function of the initial magnetic field Bi and the solenoidal field Bs

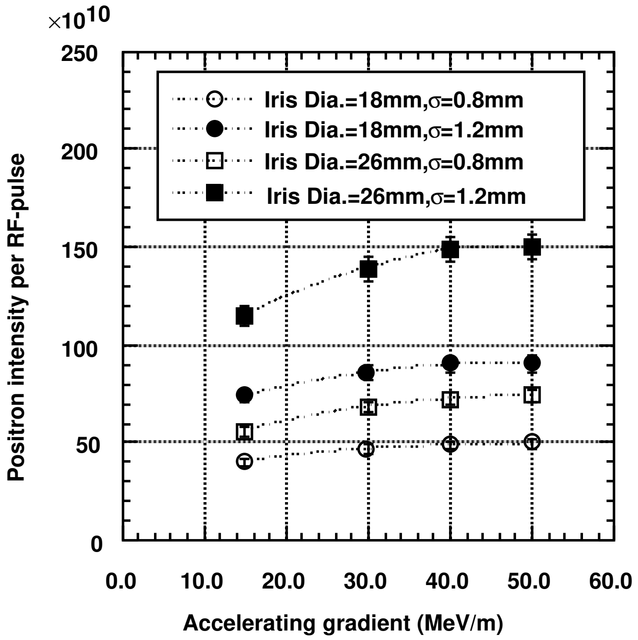

Figure 4.18: Simulated positron intensities as functions of the accelerating gradient, the iris diameter at the exit, and the incident electron beam radius.

that $Bi = 8$ T is a good compromise between the attainable positron intensity and engineering problems to be solved. Given this magnetic field, we get the highest positron intensity when μ in Eq. (4.7) is 50 m^{-1}.

Accelerating Sections with Solenoidal Field : The energies of the positrons accepted by the phase-space transformer section have a large spread of about 4 MeV, causing a slip in phase during the subsequent acceleration. Furthermore, a finite transverse momentum results in an additional phase slip, since the helical motion has a longer path length than that of straight motion down the axis. Therefore, the accelerating sections should provide a high accelerating gradient, as well as a large aperture desirable in view of the efficiency. Figure 4.18 gives the simulation result, which shows that we can achieve a high positron intensity by enlarging the incident beam radius and the iris diameter. We set the accelerating gradient at 30 MeV/m and the iris diameter at 26 mm. Consequently, the positrons acquire an energy of 90 MeV after the acceleration with two sections of a 1.5 m-long constant gradient accelerating structure in a solenoidal field of 0.8 T,

1.98 GeV Preinjector Linac : The 90 MeV positrons are accelerated up to 1.98 GeV by a S-band preinjector linac and are transported to the pre-damping ring. The linac has an accelerating gradient of 30 MeV/m provided by series of 3 m-long constant gradient accelerating structures with an iris aperture of 26 mm. In order to achieve a large transverse acceptance which matches that of the pre-damping ring, the linac should be equipped with 9 FODOs around the first accelerating structure and 3 $\sim$ 6 more around the subsequent structures. Consequently, the system realizes the transverse acceptance of 0.027 rad $\cdot$ m and an energy acceptance of ± 1 %.

Pre-Damping Ring

Main parameters of the pre-damping ring are given in Table 4.4, where the large transverse

Table 4.4: Main parameters of the JLC pre-damping ring

Energy [GeV]	1.98
Transverse acceptance [rad $\cdot$ m]	0.027
Extraction normalized emittance [rad $\cdot$ m]	0.001
Energy acceptance [%]	$\pm$ 1
Damping time [ms]	3
RF frequency [GHz]	0.714
Repetition rate [Hz]	150

acceptance of 0.027 radm should be noted. Figure 4.19 gives the simulated positron intensity as a function of the transverse acceptance at the downstream end of the accelerating sections with solenoidal field, for different values of energy acceptance. Clearly, the transverse acceptance is more important than energy acceptance. At the design transverse acceptance of 0.027 radm, 8×10^{11} positrons per RF-pulse will be obtained at the interaction point.

It has been shown that the conventional positron-production scheme shown in fig 4.14 can meet the JLC-I requirement of 8×10^{11} positrons/RF-pulse. Main parameters of the JLC-I positron source are summarized in Table 4.5. The validity of the conceptual design presented above will be confirmed at the ATF now under construction.

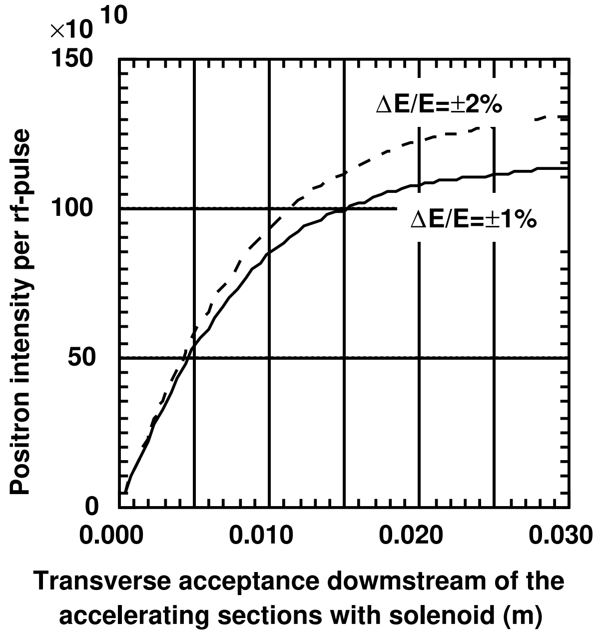

Figure 4.19: The simulated positron intensity as a function of the transverse acceptance at the downstream end of the accelerating sections with solenoidal field, for different values of energy acceptance.

Table 4.5: Main parameters of the JLC positron source Injected Electron Beam

Injected Electron Beam	
Energy [GeV]	10
Intensity [/ rf-pulse]	5.4×10^{11}
rms beam radius [mm]	1.2
Beam power [kW]	130
Target Section	
Material	W–Re
Thickness [mm]	21 (6 Radiation length)
Phase-space Transformer Section	
Initial magnetic field [T]	8
Length [mm]	180
Accelerating Section With Solenoids	
Accelerating frequency [MHz]	2856
Repetition rate [Hz]	150
Accelerating gradient [MeV/m]	30
Structure length [m]	1.5 (×2)
Iris diameter at the exit [mm]	26
Constant solenoidal field [T]	0.8
Beam Transport To Pre-damping Ring	
Transverse acceptance [rad · m]	0.027
Energy acceptance [%]	± 1